An optical lattice with sound

Yudan Guo,[1,2] Ronen M. Kroeze,[1,2] Brendan P. Marsh,[2,3] Sarang Gopalakrishnan,[4] Jonathan Keeling,[5] and Benjamin L. Lev[1,2,3]

Quantised sound waves—phonons—govern the elastic response of crystalline materials, and also play an integral part in determining their thermodynamic properties and electrical response (e.g., by binding electrons into superconducting Cooper pairs) [1-3]. The physics of lattice phonons and elasticity is absent in simulators of quantum solids constructed of neutral atoms in periodic light potentials: unlike real solids, traditional optical lattices are silent because they are infinitely stiff [4]. Optical-lattice realisations of crystals therefore lack some of the central dynamical degrees of freedom that determine the low-temperature properties of real materials. Here, we create an optical lattice with phonon modes using a Bose-Einstein condensate (BEC) coupled to a confocal optical resonator. Playing the role of an *active* quantum gas microscope, the multimode cavity QED system both images the phonons and induces the crystallisation that supports phonons via short-range, photon-mediated atom-atom interactions. Dynamical susceptibility measurements reveal the phonon dispersion relation, showing that these collective excitations exhibit a sound speed dependent on the BEC-photon coupling strength. Our results pave the way for exploring the rich physics of elasticity in *quantum* solids, ranging from quantum melting transitions [5] to exotic "fractonic" topological defects [6] in the quantum regime.

An optical lattice with sound

Yudan Guo,[1,2] Ronen M. Kroeze,[1,2] Brendan P. Marsh,[2,3] Sarang Gopalakrishnan,[4]
Jonathan Keeling,[5] and Benjamin L. Lev[1,2,3]

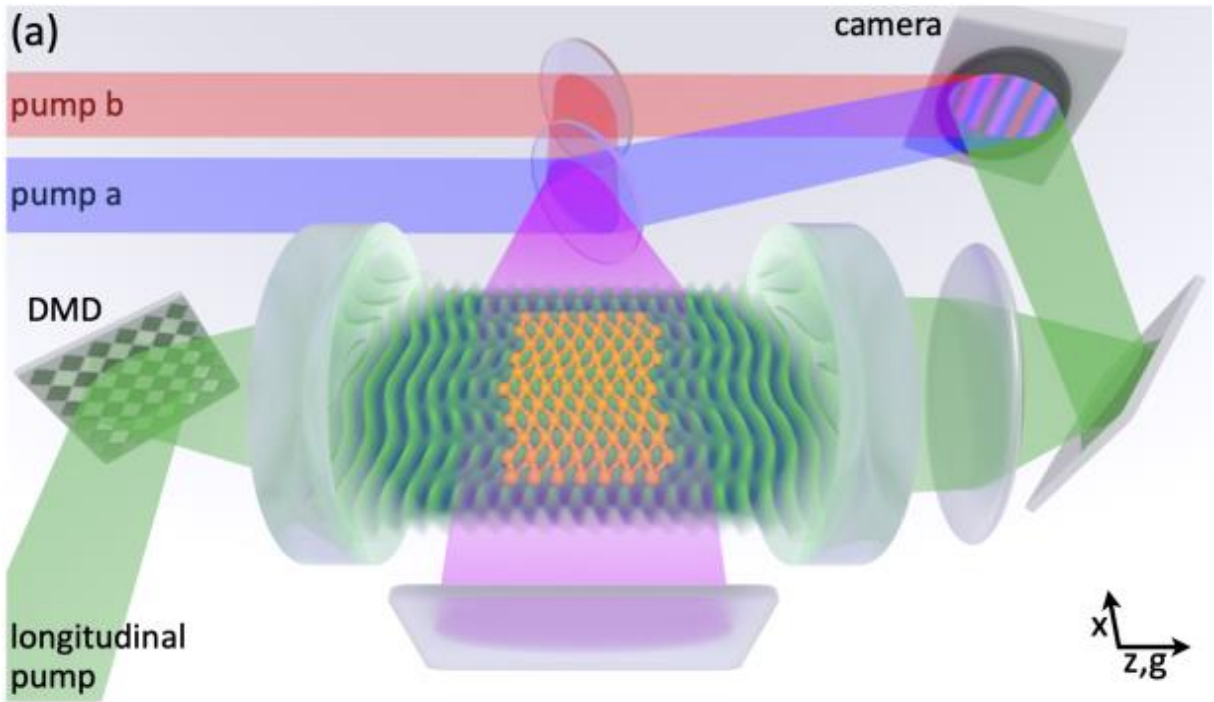

Many-body physics with ultracold gases

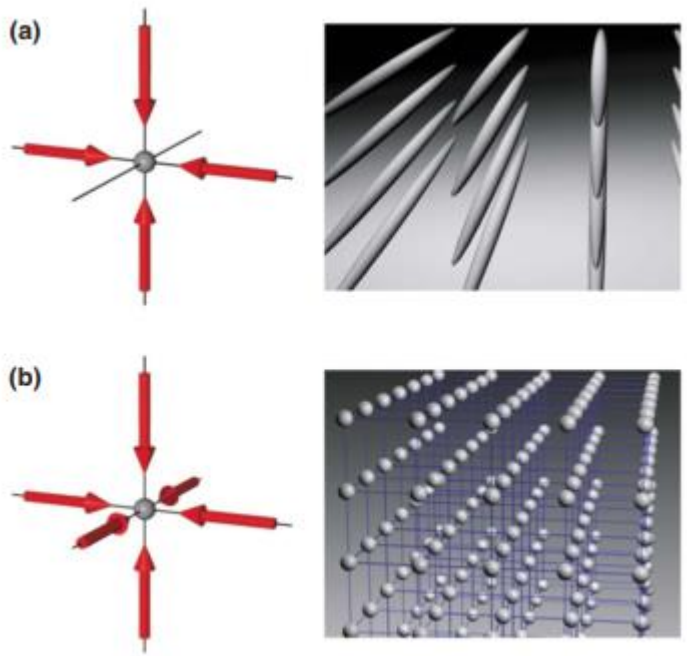

resulting optical potential is then given by the sum of three standing waves. In the center of the trap, for distances much smaller than the beam waist, the trapping potential can be approximated as the sum of a homogeneous periodic lattice potential

$$V_p(x,y,z) = V_0(\sin^2 kx + \sin^2 ky + \sin^2 kz) \qquad (36)$$

Exploring Phase Coherence in a 2D Lattice of Bose-Einstein Condensates

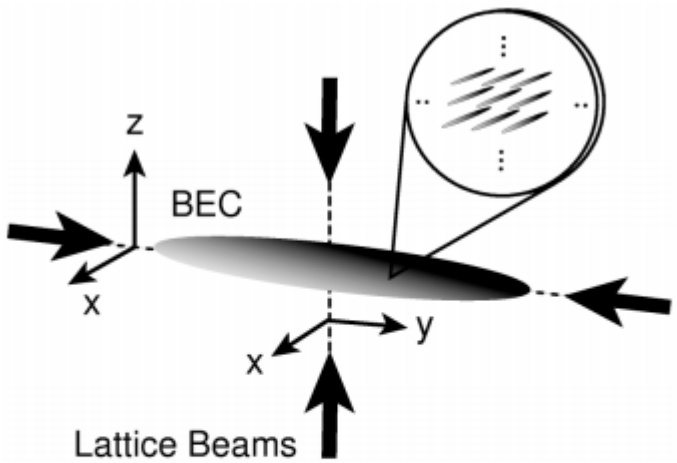

FIG. 1. Schematic setup of the experiment. A 2D lattice potential is formed by overlapping two optical standing waves along the horizontal axis (y axis) and the vertical axis (z axis) with a Bose-Einstein condensate in a magnetic trap. The condensate is then confined to an array of several thousand narrow potential tubes (see inset).

Ultracold neutral atoms confined in optical lattices have been a fruitful platform for "emulating" the itinerant motion of electrons in crystals [7]. Optical lattices, however, lack a crucial feature of real crystal lattices, which is *elasticity*. Real crystal lattices vibrate, deform in response to electrons, and transmit stresses; in contrast, optical lattices are nondynamical. Elasticity has

The primarily contact interactions among Rb do not support crystallisation. Optical cavity photons, however, can mediate interactions that do support crystallisation, as follows. We begin by considering a pump field oriented transverse to a Fabry-Pérot cavity axis that is far detuned from all but a single resonance. Above a critical threshold pump strength, a density wave (DW) polariton condensate forms via a superradiant (Hepp-Lieb-Dicke) phase transition: The N intracavity atoms cooperatively scatter pump photons into the cavity, forming a coherent optical state, while concomitantly the atoms adopt one of two chequerboard configurations of the $\lambda/2$-period lattice [13, 14]. This $\cos k_r x \cos k_r z$ lattice is formed by the interference of the pump field with the emergent cavity field. The two-photon scattering process excites the $k = 0$ BEC into a superposition of $|k_x, k_z\rangle = |\pm k_r, \pm k_r\rangle$ momentum modes, where $\hat{x}$ ($\hat{z}$) is the pump (cavity) axis, the pump and cavity fields are of wavelength $\lambda \approx 780$ nm, and $k_r = 2\pi/\lambda \approx 8$ rad/μm is the recoil momentum; $\hbar\omega_r = \hbar^2 k_r^2/2m$ is the recoil energy, approximately 3.8 kHz. The state is stable if the pump frequency ω_P is red-detuned by an amount $\Delta_C = \omega_P - \omega_C < 0$ from the cavity resonance ω_C.

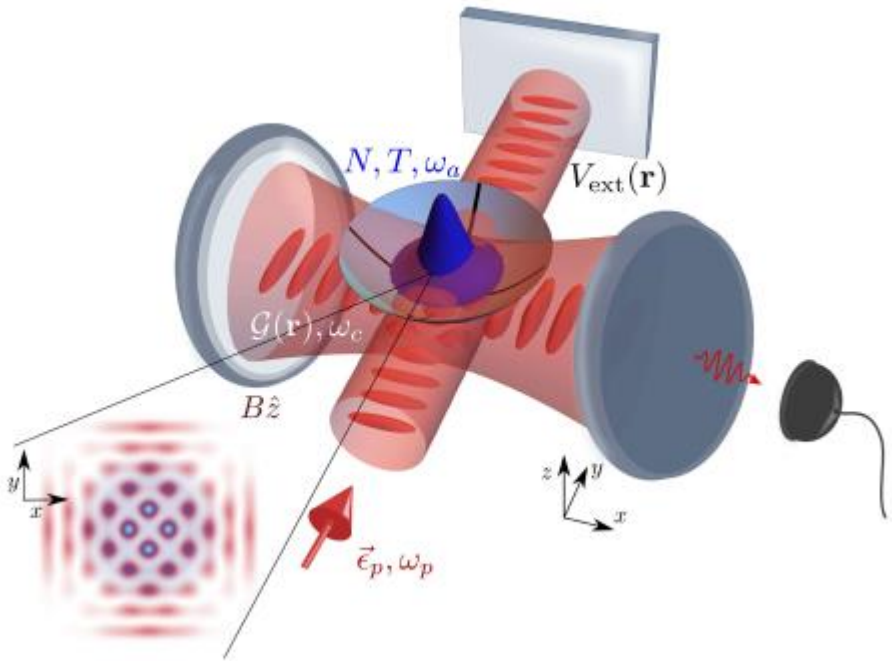

Cavity QED with Quantum Gases: New Paradigms in Many-Body Physics

Such single-mode experiments have enabled the exploration of a variety of quantum collective phenomena [15–18], but do not have a continuous translational symmetry and are thus neither rigid nor elastic. A continuous translational symmetry can be restored if one adds a second cavity mode—e.g., by using a ring-cavity geometry [19–21] or crossing two cavities [22, 23]. The free phase be-

Monitoring and manipulating Higgs and Goldstone modes in a supersolid quantum gas

Julian Léonard, Andrea Morales, Philip Zupancic, Tobias Donner,* Tilman Esslinger

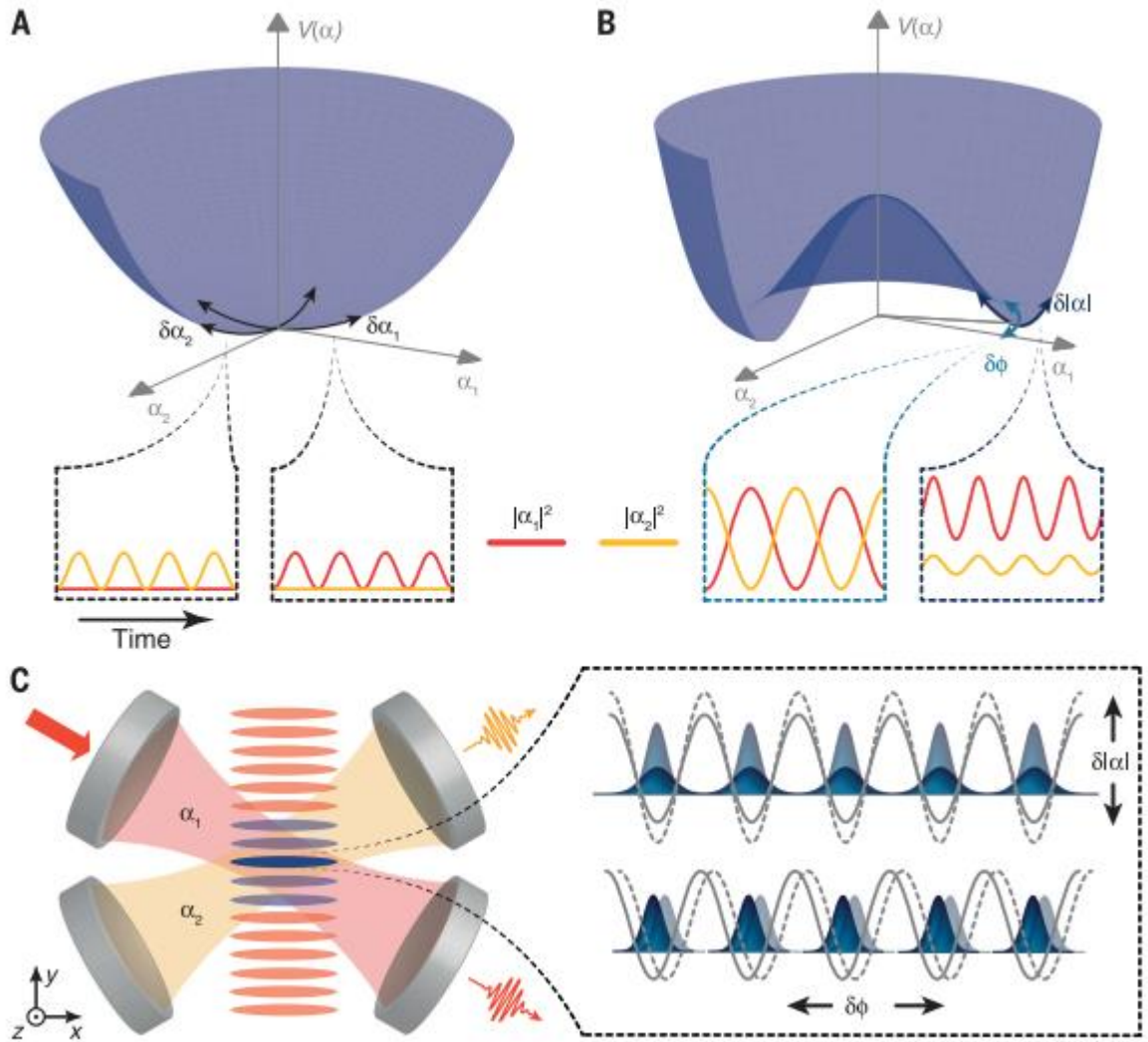

Bombeo doble – U(1) simetría

We consider two pump fields, labelled 'a' and 'b', each detuned by Δ_C from one of two cavity modes spaced one free spectral range (FSR) apart.

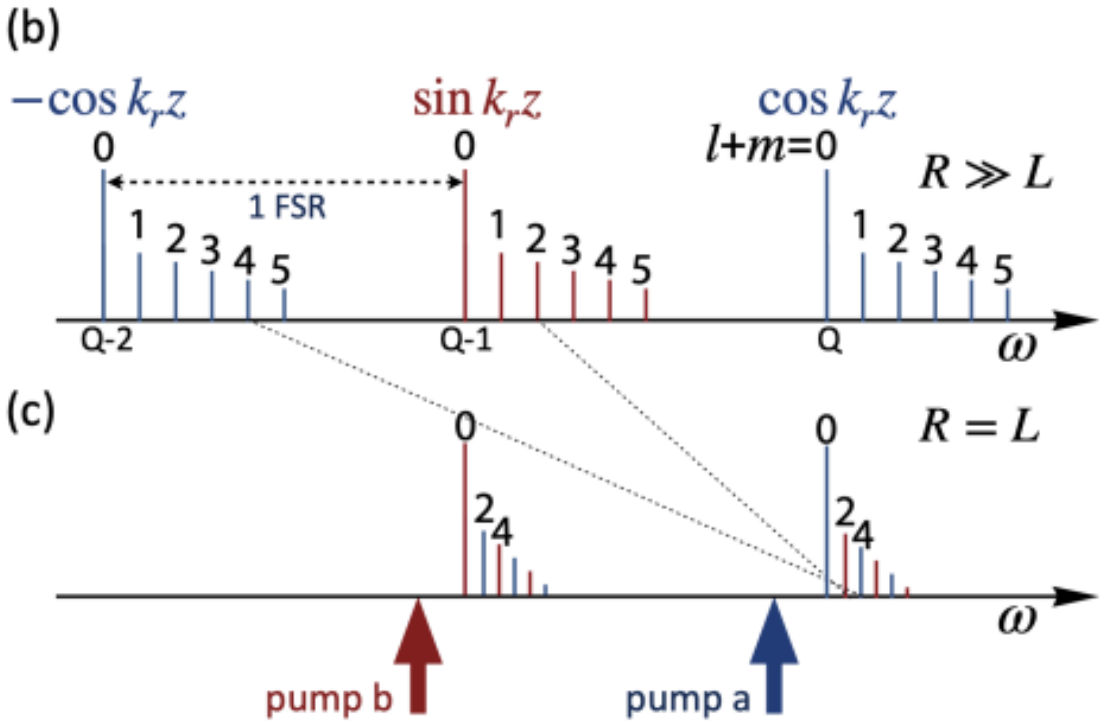

$$U^{\mathrm{sm}}_{\mathrm{total}} = U^{\mathrm{sm}} \cos[k_r(z - z')].$$

$$U^{\mathrm{mm}}_{\mathrm{total}} = U^{\mathrm{sm}} \frac{e^{-\Delta r/\xi}}{\sqrt{\Delta r/\xi}} \cos k_r \Delta z.$$

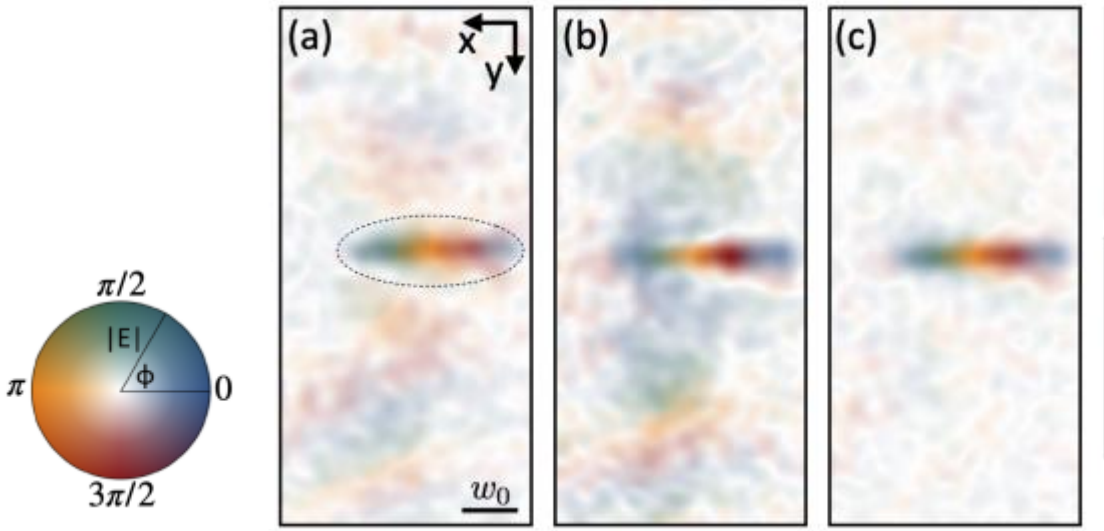

Supersolid formation in a quantum gas breaking a continuous translational symmetry

Julian Léonard[1], Andrea Morales[1], Philip Zupancic[1], Tilman Esslinger[1] & Tobias Donner[1]

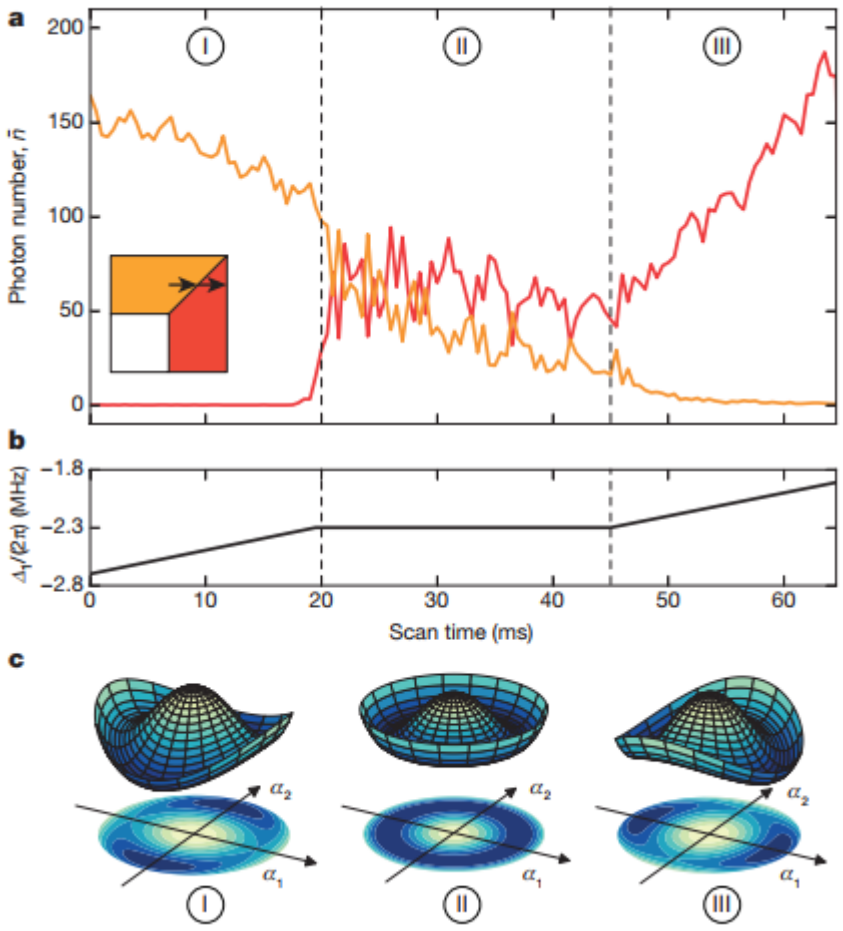

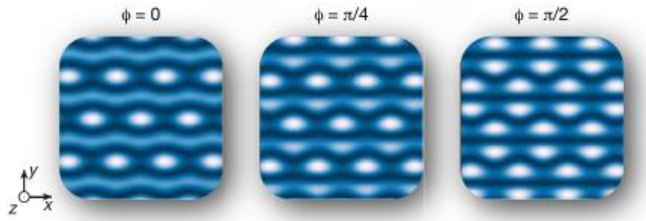

Extended Data Figure 2 | Lattice geometries for different choices of the phase ϕ of the transverse pump field for balanced cavity fields. The atoms are cut into one-dimensional lines by the strong transverse pump field. On top, spatial distributions between triangular ($\phi = 0$) and hexagonal ($\phi = \pi/2$) can form through the interference between the cavity light fields and the transverse pump, depending on the phase ϕ of the latter.

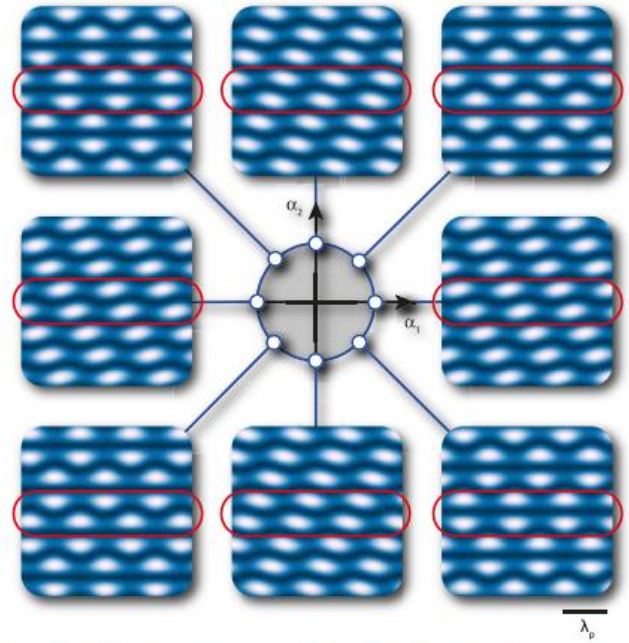

Extended Data Figure 3 | Dependence of the lattice structure on the cavity field amplitudes. The ground-state manifold for equal couplings and detunings in $\mathcal{H}$ is a circle in the space of the cavity fields α_1 and α_2. For each combination of fields, the interference potential in equation (3) between the transverse pump and cavity fields for $\phi = \pi/2$ will have its minima at different positions. Following the circle clockwise, every second line moves left (top highlighted line) while the others move right (bottom highlighted line).

Agregado de fonón

emission images in Figs. 2d,e. Like a ferromagnetic transition in the presence of an inhomogeneous longitudinal magnetic field, this breaks the underlying symmetry 'by hand,' stimulating the emergent lattice into one particular phonon mode. With no longitudinal field, the cavity emission in Figs. 2d,f reveals a linear background phase gradient, discussed in the Supplementary Information.

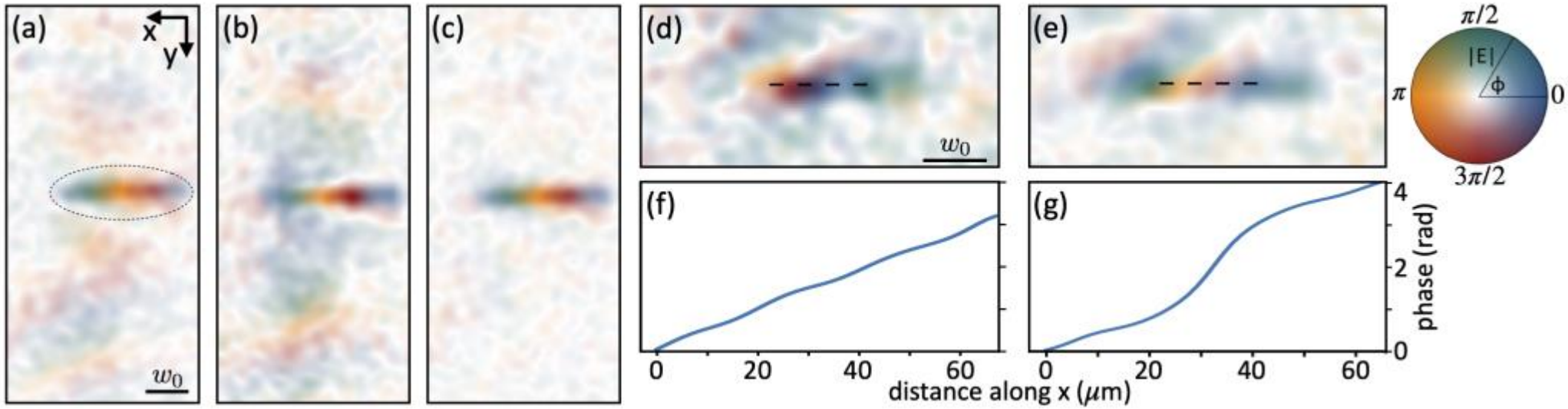

Bombeo longitudinal

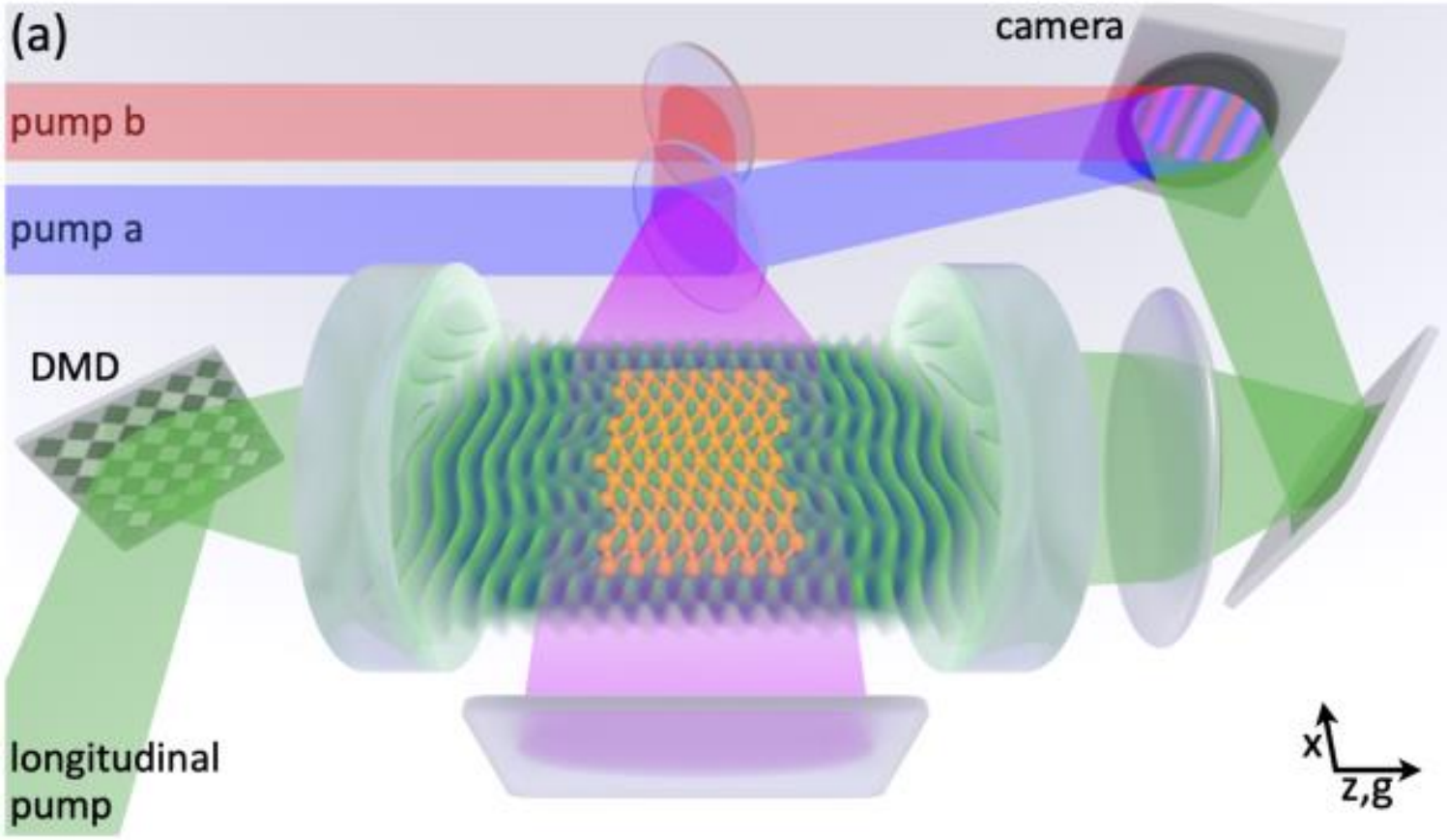

Digital micromirror devices

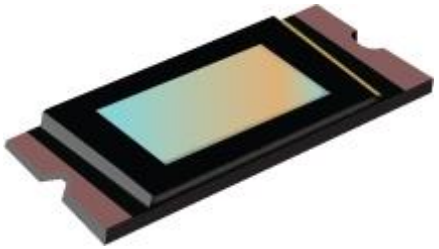

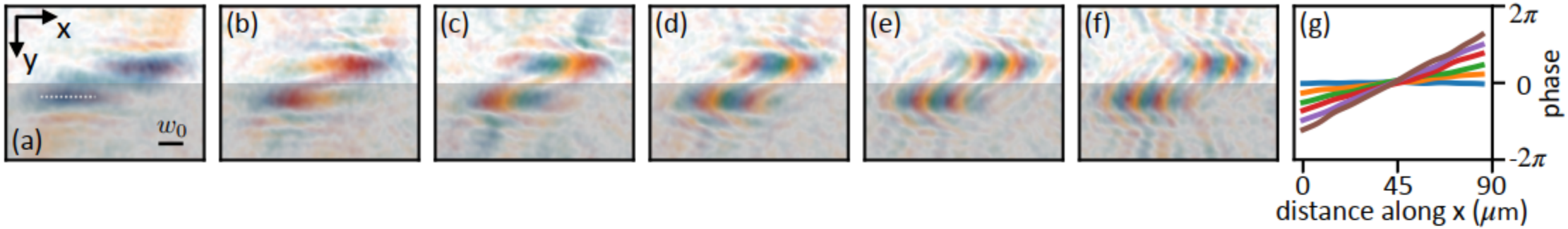

FIG. S2. Measured DMD probe transmission cavity field and their phase profile line cuts. The values of $k_\perp/k_r$ in panels (a)–(f) are $[0, 2.1, 4.2, 6.3, 8.5, 10.6] \times 10^{-3}$, respectively. The white dashed line in panel a shows the length of the cuts in panel g. Additional features around the main probe field are due to imperfections of the confocal cavity and stray light from the DMD probe beam. The grey area is the half plane that contains the mirror image of the probe field, and we do not show this redundant portion of the image in the main text figures.

to the Fourier plane of the cavity centre. Finally, any intracavity field we desire can be generated by programming its Fourier transform to be displayed on the DMD. In our experiment, we perform Bragg spectroscopy at six different momenta; the measured DMD probe fields associated with these momenta are shown in Fig. S2. The maximum $k_\perp$ modulation we can inject is limited by the numerical aperture of the lens that in-couples the DMD light and by the holding piece of the mirror.

Resultados TOF

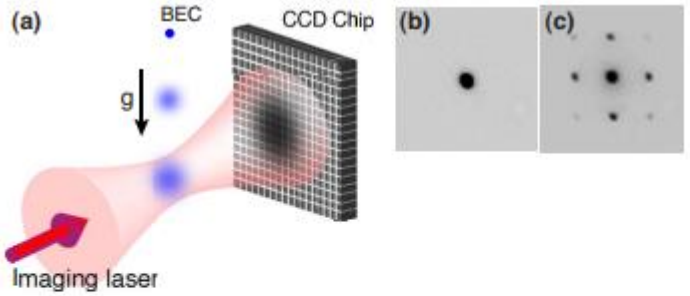

FIG. 5. (Color online) Absorption imaging. (a) Schematic setup for absorption imaging after a time-of-flight period. (b) Absorption image for a BEC released from a harmonic trap. (c) Absorption image for a BEC released from a shallow optical lattice (V_0=6E_r). Note the clearly visible interference peaks in the image.

Many-body physics with ultracold gases

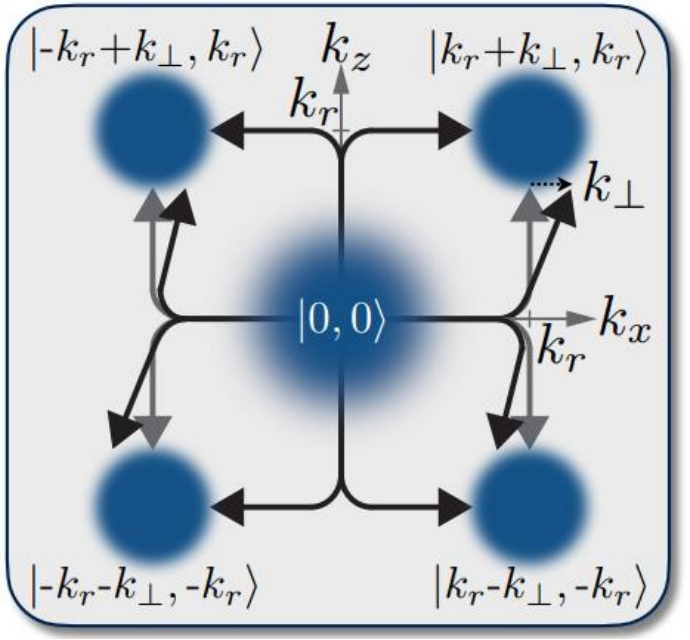

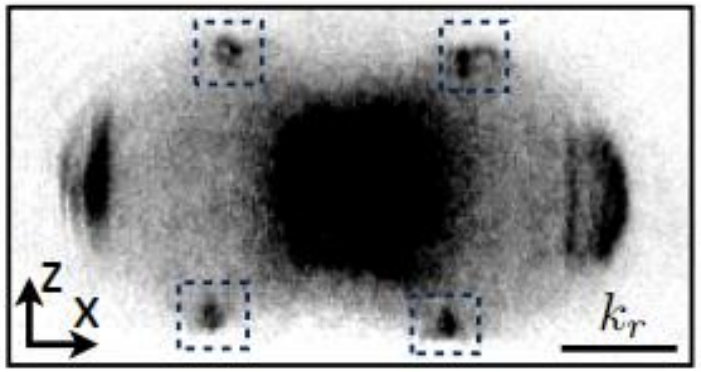

Resultados

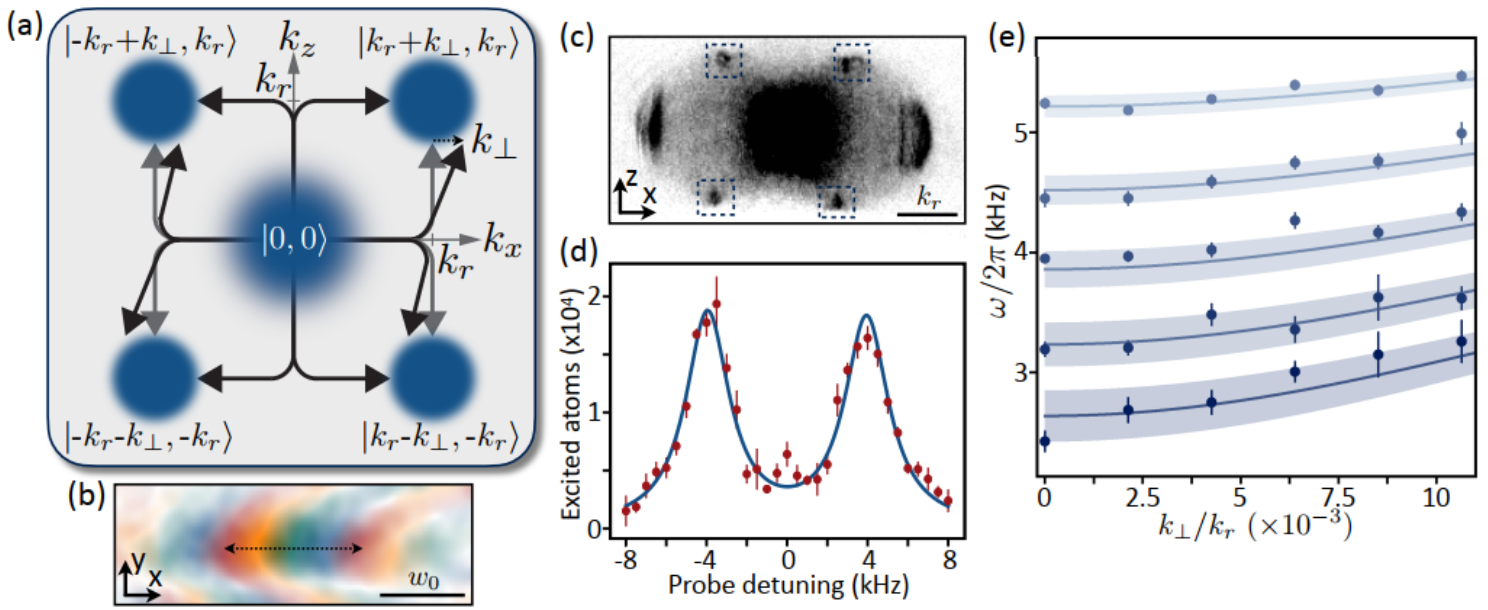

FIG. 3. **Soft-mode dispersion of density-wave polaritons below threshold.** (a) The two-photon scattering process excites atoms by receiving one momentum kick from a pump photon along $\pm\hat{x}$ and another from a cavity photon along $\pm\hat{z}$. The transverse momentum of the higher-order cavity modes shifts the $\pm\hat{x}$ momentum by an amount $\pm k_\perp$. Shown is one possible momentum state; Supplementary Information describes the others. (b) While transversely pumping below threshold, we stimulate a soft mode with a particular $k_\perp$ by seeding the cavity longitudinally. An example of a seed field is shown here, as imaged by the transmission from an empty cavity. Cavity and imaging distortions curve the $k_\perp x$ phase fronts. (c) Below-threshold absorption image of atoms in time-of-flight after a small fraction have been Bragg-stimulated into the four peaks indicated by squares. The other two peaks arise from the pump lattice alone. (d) Example Bragg scattering spectrum showing the number of scattered atoms versus probe detuning from ω_C. Data are the sum of atoms within the squares in panel (c) for $\Omega/\Omega_{\rm th} = 0.5$ and $k_\perp/k_r \approx 2.5 \times 10^{-3}$. A double Lorentzian (blue curve) is fit to the data, and the excitation energy is half the separation between peaks. Vertical bars represent standard error here and below. (e) Dispersion relation for pump strengths ranging from $\Omega/\Omega_{\rm th} = 0.3$ at the top (lightest blue) to 0.7 at bottom (darkest blue) in steps of 0.1. Each column of data at fixed $k_\perp$ shows a softening roton mode as the supermode DW polariton condenses at threshold. Data are compared to parameter-free theory curves (with error bands) derived from the theory developed in the Supplementary Information.

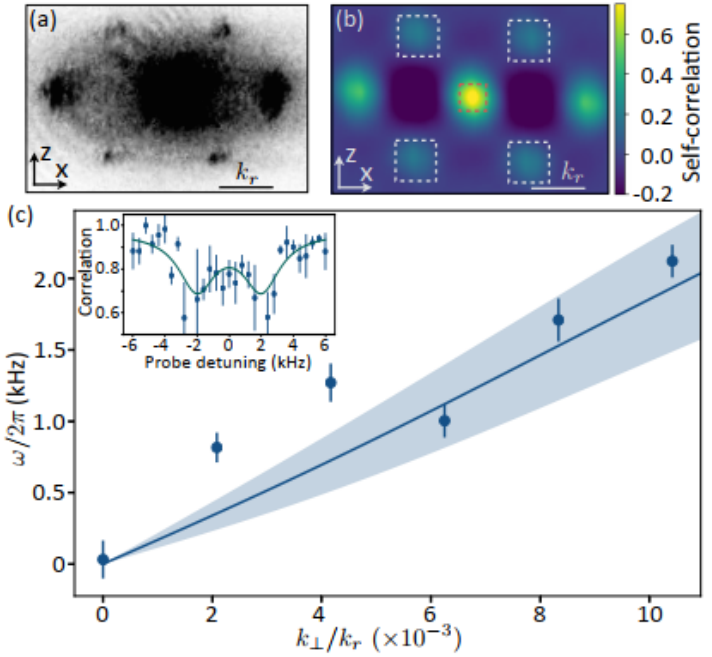

FIG. 4. **Goldstone dispersion relation** $\omega(k_\perp)$. (a) Example above-threshold time-of-flight image recording the momentum distribution $\rho(k)$. (b) The self-correlation analysis yielding $\langle\rho(k+\delta k)\rho(k)\rangle$. The white dashed squares indicate regions of interest for extracting the correlation strength associated with the chequerboard lattice. The correlation strength is calculated by normalising the sum of the values in white squares by that in the central red dashed square. (c) The dispersion relation curve (blue) is overlaid using the theory presented in the Supplemental Information and is parameter-free. The data are consistent with a linear dispersion for $k_\perp \ll \zeta$. The pump strength is $\Omega/\Omega_{\rm th} = 1.25$. The error band (light blue) represents one-sigma error in the theory parameters. Inset shows an example dynamic susceptibility spectrum obtained from self-correlation analyses taken for $k_\perp/k_r \approx 0.01$. Correlations decrease on resonance because the momentum structure factor differs from the $|0,0\rangle$ state due to the addition of $k_\perp$.

Recientes

Fluorescence Detection of a Trapped Ion with a Monolithically Integrated Single-Photon-Counting Avalanche Diode

W. J. Setzer,[1,a)] M. Ivory,[1] O. Slobodyan,[1] J. W. Van Der Wall,[1] L. P. Parazzoli,[1] D. Stick,[1] M. Gehl,[1] M. Blain,[1] R. R. Kay,[1] and H. McGuinness[1]
Sandia National Laboratories, Albuquerque, New Mexico 87185, USA

(Dated: 5 May 2021)

We report on the first demonstration of fluorescence detection using single-photon avalanche photodiodes (SPADs) monolithically integrated with a microfabricated surface ion trap. The SPADs are positioned below the trapping positions of the ions, and designed to detect 370 nm photons emitted from single $^{174}Yb^{+}$ and $^{171}Yb^{+}$ ions. We achieve an ion/no-ion detection fidelity for $^{174}Yb^{+}$ of 0.99 with an average detection window of 7.7(1) ms. We report a dark count rate as low as 1.2 kHz at room temperature operation. The fidelity is limited by laser scatter, dark counts, and heating that prevents holding the ion directly above the SPAD. We measure count rates from each of the contributing sources and fluorescence as a function of ion position. Based on the active detector area and using the ion as a calibrated light source we estimate a SPAD quantum efficiency of 24±1%.

Recientes

Article

Shaping Dynamical Casimir Photons

Diego A. R. Dalvit [1]* and Wilton J. M. Kort-Kamp [2]

[1] Los Alamos National Laboratory, MS B213, Los Alamos, NM 87545, USA; dalvit@lanl.gov
[2] Los Alamos National Laboratory, MS B262, Los Alamos, NM 87545, USA; kortkamp@lanl.gov
* Correspondence: dalvit@lanl.gov

Abstract: Temporal modulation of the quantum vacuum through fast motion of a neutral body or fast changes of its optical properties is known to promote virtual into real photons, the so-called dynamical Casimir effect. Empowering modulation protocols with spatial control could enable to shape the spectral, spatial, spin, and entanglement properties of the emitted photon pairs. Space-time quantum metasurfaces have been proposed as a platform to realize this physics via modulation of their optical properties. Here, we report the mechanical analog of this phenomenon by considering systems whose lattice structure undergoes modulation in space and in time. We develop a microscopic theory that applies both to moving mirrors with modulated surface profile and atomic array meta-mirrors with perturbed lattice configuration. Spatio-temporal modulation enables motion-induced generation of steered frequency-path entangled photon pairs in co- and cross-polarized states, as well as vortex photon pairs featuring frequency-angular momentum entanglement. The proposed space-time dynamical Casimir effect can be interpreted as an induced dynamical asymmetry in the quantum vacuum.

Keywords: Dynamical Casimir Effect; Spatio-temporal modulation; Quantum metasurfaces

Recientes

Gravitational redshift tests with atomic clocks and atom interferometers

Fabio Di Pumpo,[1,*] Christian Ufrecht,[1] Alexander Friedrich,[1] Enno Giese,[2,1,3] Wolfgang P. Schleich,[1,4,5,6] and William G. Unruh[5,7]

[1] *Institut für Quantenphysik and Center for Integrated Quantum Science and Technology (IQ^{ST}), Universität Ulm, Albert-Einstein-Allee 11, D-89069 Ulm, Germany*
[2] *Institut für Angewandte Physik, Technische Universität Darmstadt, Schlossgartenstr. 7, D-64289 Darmstadt, Germany*
[3] *Institut für Quantenoptik, Leibniz Universität Hannover, Welfengarten 1, D-30167 Hannover, Germany*
[4] *Institute of Quantum Technologies, German Aerospace Center (DLR), Söflinger Straße 100, D-89077 Ulm, Germany*
[5] *Hagler Institute for Advanced Study and Department of Physics and Astronomy, Institute for Quantum Science and Engineering (IQSE), Texas A&M University, College Station, Texas 77843-4242, USA*
[6] *Texas A&M AgriLife Research, Texas A&M University, College Station, Texas 77843-4242, USA*
[7] *Department of Physics and Astronomy, University of British Columbia, Vancouver, British Columbia V6T 1Z1, Canada*

Atomic interference experiments can probe the gravitational redshift via the internal energy splitting of atoms and thus give direct access to test the universality of the coupling between matter-energy and gravity at different spacetime points. By including possible violations of the equivalence principle in a fully quantized treatment of all degrees of freedom, we characterize how the sensitivity to gravitational redshift violations arises in atomic clocks and atom interferometers, as well as their underlying limitations. Specifically, we show that: (i.) Contributions beyond linear order to trapping potentials lead to such a sensitivity of trapped atomic clocks. (ii.) While Bragg-type interferometers, even with a superposition of internal states, with state-independent, linear interaction potentials are at first insensitive to gravitational redshift tests, modified configurations, for example by relaunching the atoms, can mimic such tests tests under certain conditions. (iii.) Guided atom interferometers are comparable to atomic clocks. (iv.) Internal transitions lead to state-dependent interaction potentials through which light-pulse atom interferometers can become sensitive to gravitational redshift violations.